Potential Oscillations in Galvanostatic Electrooxidation of Formic Acid on Platinum: A Time-Resolved Surface-Enhanced Infrared Study

Gabor Samjeské,[†,‡] Atsushi Miki,[‡] Shen Ye,[‡] Akira Yamakata,[‡] Yoshiharu Mukouyama,[§] Hiroshi Okamoto,[§] and Masatoshi Osawa*[,†,‡]

CREST, Japan Science and Technology Agency, Kawaguchi, Saitama 332-0012, Japan, Catalysis Research Center, Hokkaido University, Sapporo 001-0021, Japan, and College of Science and Engineering, Tokyo Denki University, Hatoyama, Saitama 350-0394, Japan

Received: September 15, 2005; In Final Form: October 17, 2005

The mechanism of temporal potential oscillations that occur during galvanostatic formic acid oxidation on a Pt electrode has been investigated by time-resolved surface-enhanced infrared absorption spectroscopy (SEIRAS). Carbon monoxide (CO) and formate were found to adsorb on the surface and change their coverages synchronously with the temporal potential oscillations. Isotopic solution exchange (from $H^{13}COOH$ to $H^{12}COOH$) and potential step experiments revealed that the oxidation of formic acid proceeds dominantly through adsorbed formate and the decomposition of formate to CO_2 is the rate-determining step of the reaction. Adsorbed CO blocks the adsorption of formate and also suppresses the decomposition of formate to CO_2, which raises the potential to maintain the applied current. The oxidative removal of CO at a high limiting potential increases the coverage of formate and accelerates the decomposition of formate, resulting in a potential drop and leading to the formation of CO. This cycle repeats itself to give the sustained temporal potential oscillations. The oscillatory dynamics can be explained by using a nonlinear rate equation originally proposed to explain the decomposition of formate and acetate on transition metal surfaces in UHV.

1. Introduction

Electrochemical reaction systems can exhibit interesting nonlinear dynamic behaviors such as periodic oscillations, quasiperiodicities, and chaos.[1] The electrooxidation of formic acid on Pt and Pt-group metals is a typical system showing periodic oscillations. In potentiostatic (i.e., constant potential) systems the current can oscillate and in galvanostatic (i.e., constant current) systems the potential can oscillate. Despite extensive experimental and theoretical studies,[1,2] the mechanism of the oscillations has not been fully understood yet.

It is widely accepted that the electrooxidation of formic acid to CO_2 follows the so-called "dual-pathway" mechanism.[3] One path involves a fast reaction via a reactive intermediate (direct path) and the second path includes a step in which a poisoning intermediate is formed (indirect path). Infrared reflection−absorption spectroscopy (IRAS) has clearly shown that CO produced by dehydration of formic acid

$$HCOOH + * \rightarrow CO(a) + H_2O \quad (1)$$

is the poisoning species,[4] where the asterisk and "(a)" stand for a vacant surface site and adsorbed species, respectively. Adsorbed CO is oxidized to CO_2 at high potentials by the reaction with surface bonded OH as

$$H_2O + * \rightleftharpoons OH(a) + H^+ + e^- \quad (2)$$

$$CO(a) + OH(a) \rightarrow CO_2 + H^+ + e^- + 2* \quad (3)$$

or with an adsorbed water molecule as

$$H_2O + * \rightleftharpoons H_2O(a) \quad (4)$$

$$CO(a) + H_2O(a) \rightarrow CO_2 + 2H^+ + 2e^- + 2* \quad (5)$$

On the other hand, the reactive intermediate in the direct path has not yet been identified definitely. So far, a carboxylic acid species adsorbed on the electrode surface with carbon atom (COOH) has been assumed to be the reactive intermediate and the direct path has tentatively been written as

$$HCOOH + * \xrightarrow{rds} \underline{C}OOH(a) + H^+ + e^- \quad (6)$$

$$\underline{C}OOH(a) \xrightarrow{fast} CO_2 + H^+ + e^- \quad (7)$$

where "rds" stands for the rate-determining step.

Both potential and current oscillations have been explained basically in terms of the dual-path mechanism.[1,2] Albahadily and Schell[2e] explained the potential oscillations under galvanostatic conditions as follows: Adsorbed CO blocks the direct path, which results in an increase in the potential to maintain the applied current. The adsorbed CO is removed from the surface through reaction 3 (feedback step) at potentials high enough for the OH formation, which results in the potential drop and the cycle repeats itself to give temporal oscillations. Some modified mechanistic models which include the oxidation of the electrode surface,[2a,c] the change of pH at the interface,[2d,h] and the adsorption of OH and anions[2i,j,m] have also been proposed on the basis electrochemical and physicochemical measurements.

* Address correspondence to this author. E-mail: osawam@cat.hokudai.ac.jp.
† CREST, Japan Science and Technology Agency.
‡ Hokkaido University.
§ Tokyo Denki University.

10.1021/jp055220j CCC: $30.25
Published on Web 11/18/2005

In parallel to the experimental approaches, the oscillatory behaviors have been examined also by mathematical modeling. Wojtowicz et al.[2a] proposed an autocatalytic surface-oxide removal step for the feedback step in the oscillations and suggested that the oscillations can be modeled by nonlinear kinetic equations for formic acid oxidation. Albahadily and Schell[2e] succeeded in simulating galvanostatic potential oscillations by assuming nine or ten possible surface reaction steps (which requires six or seven parameters). On the other hand, Okamoto and co-workers[2f,g,k] showed that potential oscillations can be simulated with only three parameters by assuming the potential dependence of the adsorption/desorption of H_2O and of the oxidation of CO with adsorbed H_2O, eqs 4 and 5. Strasser et al.[2i,j] simulated potentiostatic current oscillations assuming that the adsorption of OH blocks the active sites for the direct path. Such mathematical modeling can give some information about the electrode dynamics that is not easily accessible by experiments. Nevertheless, it should be noted that all these mathematical models can simulate observed oscillations satisfactorily despite different assumptions of elementary steps and chemical species involved. This indicates the necessity of further detailed study of the reaction dynamics occurring at the electrode surface during the oscillations.

The identification of the surface bonded species involved in the reaction is essential for elucidating the mechanisms of formic acid oxidation and the oscillations. Infrared spectroscopy is suited for this purpose. Unfortunately, however, IRAS, the most standard in situ surface infrared spectroscopy technique,[5] is not very suitable for dynamic monitoring of electrode reactions due to several problems such as limited mass transfer and high cell resistance arising from the use of thin-layer spectroelectrochemical cells. In the present study, we have examined the potential oscillation dynamics by using an alternative surface infrared spectroscopy technique, surface-enhanced infrared absorption spectroscopy (SEIRAS) in a Kretschmann-type attenuated-total-reflection (ATR) mode[6] because of its several advantages over IRAS: free mass transport, quick response of the electrochemical system, less spectral interference from the bulk solution, and higher sensitivity (10 times or more).[6] These advantages facilitate the real-time monitoring of the oscillations with enough time resolutions. We will show in this report that formate (HCOO) adsorbed in a bridging configuration (bonded via both oxygen atoms to two surface sites) is a reactive intermediate in the direct path of formic acid oxidation and propose a new mechanism of potential oscillations on the basis of the experimental results.

2. Experimental Section

The details of ATR-SEIRAS experiments have been described elsewhere.[6−8] Two spectroelectrochemical cells were used. The cell used in the most experiments was a glass one with a cell volume of 20 mL.[7b] The other was a flow cell made of Kel-F with a smaller volume (1.5 mL), which was used in isotopic substitution experiments ($H^{12}COOH/H^{13}COOH$) for identifying reaction intermediates. A Pt-mesh and a reversible hydrogen electrode (RHE) served as the counter and reference electrodes, respectively. Potential and galvanostatic controls were done with an EG&G 263A potentiostat/galvanostat in combination with an M270 software package (Princeton Applied Research).

The working electrode was a thin Pt film chemically deposited on the totally reflecting plane of a hemicylindrical Si ATR prism (1 cm in diameter and 2.5 cm long, Nippon Pastec, Osaka). The procedures of the Pt deposition were described elsewhere.[8] The Pt-coated prism was attached to the cell via an O-ring (i.d. = 15 mm). The electrode surface was cleaned by repeating potential sweeps between 0.05 and 1.5 V in 0.5 M H_2SO_4 before every set of experiment.

SEIRA spectra were recorded on a Bio-Rad FTS-60A/896 FT-IR spectrometer equipped with an MCT detector and a homemade single-reflection accessory (incident angle of 70°). The spectrometer was operated in the rapid-scan kinetic mode (40 kHz) with a spectral resolution of 4 cm^{-1} and a suitable time resolution ranging from 80 ms to 1 s. To obtain *absolute* spectra, a reference spectrum of the clean electrode surface (R_0) was collected first in the supporting electrolyte without formic acid and then sample spectra (R) were collected after adding formic acid into the cell to a desired concentration (0.1 or 1 M). All spectra are shown in the absorbance units defined as $A = -\log(R/R_0)$. The spectrometer scan was started at the same time with electrochemical measurements.

The electrolyte solution used was a 0.5 M H_2SO_4 prepared from ultrapure Millipore water and H_2SO_4, which was deaerated with Ar before and during measurements. All chemicals, H_2SO_4 (Suprapur, Merck), HCOOH (99%, Wako Chemicals), and $H^{13}COOH$ (99%, Cambridge Isotope Laboratories), were used as received without further purification. All measurements were carried out at room temperature (∼25 °C).

3. Results and Discussion

3.1. Electrochemical Characterization of the Pt Electrode. The chemically deposited Pt electrode was as shiny as well-polished bulk Pt electrodes and its fundamental electrochemical behavior was identical with that of polycrystalline Pt electrodes.[8] The real surface area of the electrode estimated from the charge for hydrogen adsorption/desorption in 0.5 M H_2SO_4 was 10.8 cm^2 assuming a charge of 210 $\mu C\ cm^{-2}$ for full monolayer hydrogen adsorption, while the geometrical surface area of the electrode contacting with the solution was 1.77 cm^2. The large roughness factor of 6.1 (=10.8 cm^2/1.77 cm^2) arises from the surface roughness in the nanometer scale.[8b] The nanometer-scale roughness facilitates the interaction of the incident infrared photons with the metal and adsorbed species, resulting in SEIRA.[6,9] The electrode was stable enough and no change in surface area was observed within experimental errors after spectroelectrochemical measurements.

3.2. Potential Oscillations under Galvanostatic Conditions. A typical oscillation pattern in 0.5 M H_2SO_4 + 1 M HCOOH solution at a constant current of 10 mA is shown in Figure 1a. Only the data after stable oscillations being established are shown for clarity. The oscillation is characterized by an initial slow rise of potential from 0.52 to about 0.6 V followed by a sharp rise to 0.8 V and a sudden drop to 0.52 V. The cycle repeats at every 2.5 s.

A series of SEIRA spectra recorded simultaneously with the potential−time curve is shown in Figure 1b. The time resolution used was 80 ms and no interferogram coaddition was employed. A spectrum collected at 0.1 V in the supporting electrolyte without formic acid was used as the reference. Five bands are found at 2030−2050, ∼1830, 1720, 1620 (negative peak), and 1323 cm^{-1} in the spectral range of 2200−1200 cm^{-1}. The bands at 2030−2050, ∼1830, and 1323 cm^{-1} are seen to change their intensities and/or peak positions periodically. These bands are assigned, from higher to lower wavenumbers, to the C−O stretching modes of linearly- and bridge-bonded CO (CO_L and CO_B, respectively),[4] and the symmetric O−C−O stretching mode of formate (HCOO) adsorbed on the surface in a bridging conformation (that is, bonded via both oxygen atoms to two surface sites).[10] Note that formate is different from COOH in

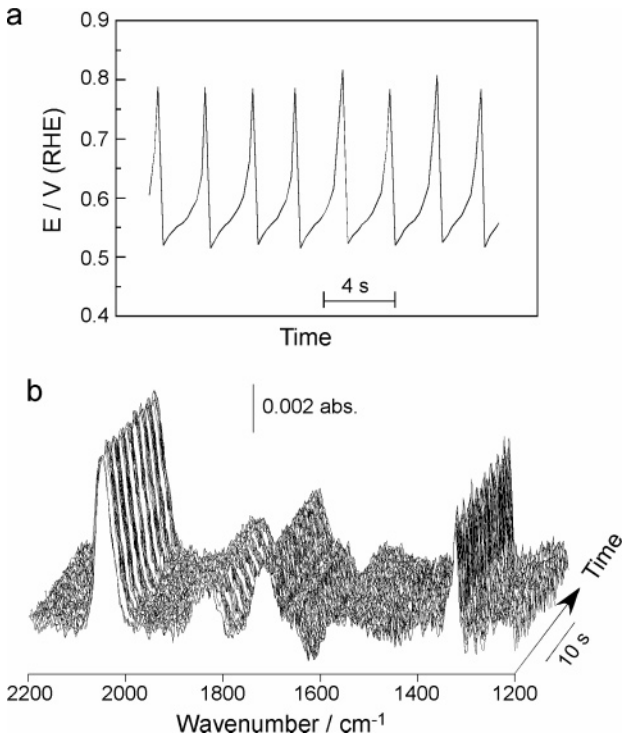

Figure 1. (a) Typical oscillation pattern observed in galvanostatic oxidation of formic acid on a polycrystalline Pt electrode in 0.5 M H_2SO_4 + 1 M HCOOH for an applied current of 10 mA and (b) a series of time-resolved SEIRA spectra of the electrode surface acquired simultaneously with the time−potential curve with a time resolution of 80 ms.

molecular structure. Due to the surface selection rule in SEIRAS,[6,9] which is the same as that in IRAS,[5] the antisymmetric O−C−O stretching mode of formate that gives a dipole change perpendicular to its C_2 rotating axis is not observed in the expected region (~1570 cm^{-1}) consistent with the bridging comformation.

The 1720- and 1620-cm^{-1} bands that do not change intensities are assigned to the C═O stretching mode of formic acid in the solution[8a] and the bending mode of interfacial water,[7b] respectively. Since water molecules are repelled from the interface by the adsorption of CO and formate, the water band is observed as a negative peak. The characteristic S−O stretching modes of adsorbed (bi)sulfate around 1100 and 1200 cm^{-1} [11] were observed as strong as the formate band in the pure electrolyte, but hardly observed under the oscillation, indicating that CO and formate is adsorbed more strongly than (bi)sulfate. An independent experiment showed that formate is not adsorbed on the Pt electrode fully covered with CO. That is, the adsorption of the species observed by IR is in the order of CO > formate > (bi)sulfate > water.

The oscillation frequency was affected by experimental conditions, especially by the applied current. The frequency of the potential oscillations decreased with decreasing applied current. The potential−time curve for an applied current of 3.2 mA is shown in Figure 2a. The potential oscillates between 0.5 and 0.8 V at every 80 s. The oscillation pattern is essentially identical with that observed at 10 mA, but the lower potential region is much longer for the smaller applied current. The corresponding SEIRA spectra are shown in Figure 3. A lower time resolution of 1 s was employed in the measurement to enhance the signal-to-noise ratio of the spectra by coadding interferograms. Since the spectral features were essentially identical with those observed at 10 mA (Figure 1b) except for

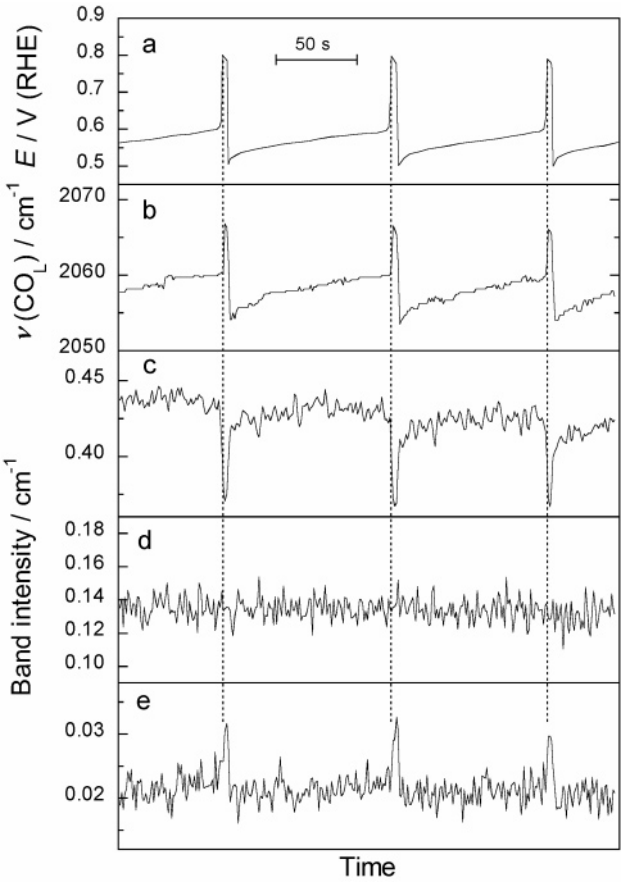

Figure 2. Oscillation pattern for an applied current of 3.2 mA (a) and spectral data taken from Figure 3 plotted as a function of time (b−e). Peak position of the CO_L band (b) and integrated band intensities of CO_L (c), CO_B (d), and formate (e). Experimental conditions were the same as in Figure 1 except for the applied current.

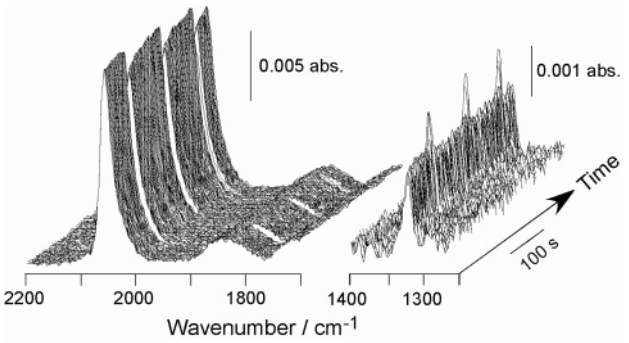

Figure 3. Series of time-resolved SEIRA spectra acquired simultaneously with the potential−time curve in Figure 2a. Time resolution was 0.98 s. Only the spectral range of the CO_L, CO_B, and formate are shown for clarity.

intensities, the limited spectral ranges involving the CO and formate bands are shown for clarity.

To find the correlations between the potential oscillations and the spectral changes, the peak frequency of CO_L and the integrated band intensities of the three adsorbates in Figure 3 are plotted in Figure 2 as a function of time. The frequency of the CO_L vibration oscillates between 2055 and 2067 cm^{-1} reflecting the potential change (panel b). The potential dependent shift of this band has been explained by the Stark tuning effect and/or electron back-donation from the metal to the $2\pi^*$ antibonding orbital of CO.[5] The coincidence of the peaks in the potential−time and frequency−time plots ensures the

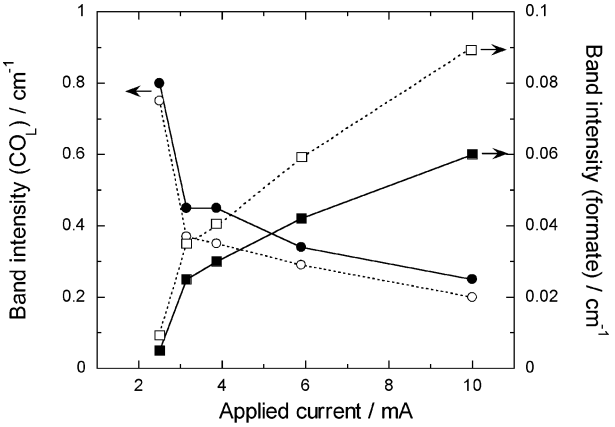

Figure 4. Applied current dependence of the higher and lower limits of the integrated band intensities of the CO_L (circles) and formate (squares) in the potential oscillations. Closed and open symbols correspond to the data at the lowest and highest potentials, respectively. Solution: 0.5 M H_2SO_4 + 1 M HCOOH.

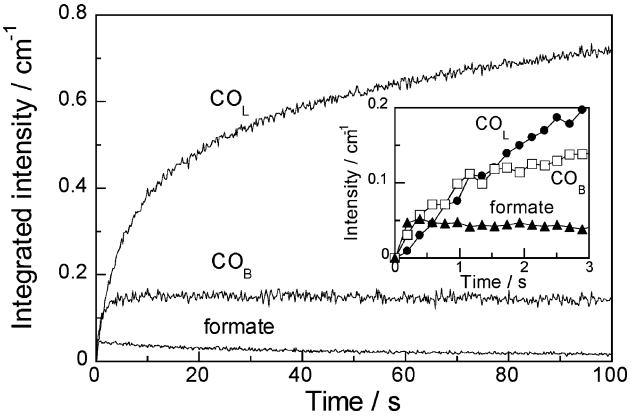

Figure 5. Integrated band intensities of CO_L, CO_B, and formate plotted as a function of time after stepping the electrode potential from 1.4 to 0.4 V in 0.5 M H_2SO_4 + 0.1 M HCOOH. Time resolution was 0.2 s.

synchronization of the electrochemical and spectroscopic measurements. The temporal changes of the band intensities of CO_L and formate (panels c and e, respectively) are also well synchronized with the potential oscillations: The CO_L band decreases and the formate band increases in intensity at the potential spikes. Potential drops when the CO_L intensity reaches its minimum and the formate intensity reaches its maximum. After the drop of the potential to the low limiting value, the formate band decreases quickly to the initial intensity, while the CO_L band recovers its intensity quickly first and then gradually. On the other hand, the CO_B band hardly changes its intensity during the oscillations (panel d), but shows a peak shift as CO_L (see Figure 3). The formate band showed no peak shift within the experimental accuracy (4 cm^{-1}).

The intensities of the CO_L and formate bands depend on the applied current. The upper and lower limits of the intensities of the two bands are plotted in Figure 4 as a function of the applied current. As the applied current is increased, the CO_L band decreases and the formate band increases in intensity. On the other hand, the CO_B band intensity was independent of the applied current (data not shown). The result shows that the changes of the CO and formate coverages are rather small in the oscillations.

3.3. Estimation of Adsorbate Coverage. For the latter discussion and also for the mathematical modeling of the potential oscillations that will be reported in a separate paper,[12] coverages (θs) of the three adsorbed species are roughly estimated from the infrared data by assuming a linear relationship between the band intensity and coverage. This assumption is reasonable at least for CO_L.[4a,13] Coverage is defined in this report as the ratio of the number of adsorbed species to that of surface atoms. The integrated band intensities of CO_L and CO_B at full CO coverage established by CO-gas bubbling (1 and 0.25 cm^{-1}, respectively) are used as the references. The CO coverage at saturation calculated from the charge required for its complete oxidation was 0.83, but the adsorption of hydrogen was totally suppressed. Taking into account the requirement of two Pt surface atoms for CO_B, the coverages of CO_L and CO_B are assumed to be 0.66 and 0.17, respectively ($\theta_{CO} = 0.66 + 0.17 = 0.83$ and $\theta_{CO\_L} + 2\theta_{CO\_B} = 1$). The higher (lower) limits of CO_L, θ_{CO-L}, in the oscillations for the applied currents of 3.2 and 10 mA are calculated by this procedure to be ~0.3 (~0.25) and ~0.2 (~0.1), respectively. Similarly, CO_B coverage is estimated to be ~0.1 independent of applied current.

For the estimation of formate coverage, the formate band intensity of 0.053 cm^{-1} at $\theta_{formate} \approx 0.14$, which will be evaluated from the isotopic substitution experiment described in section 3.6, was used as the reference. The higher (lower) limits of $\theta_{formate}$ for the applied currents of 3.2 and 10 mA are calculated to be ~0.1 (~0.05) and ~0.2 (~0.15), respectively. The estimation suggests that the electrode surface is not fully covered by CO and formate. For the applied current of 3.2 mA, for example, the coverage of surface site free of CO and formate ($=1-\theta_{CO\_L} - 2\theta_{CO\_B} - 2\theta_{formate}$) remains almost constant at about 0.4 during the oscillations.

3.4. Kinetics of CO Formation. The observed oscillations are accompanied by the formation and oxidative removal of CO_L (Figure 2). The adsorption of CO blocks the active sites for the direct path and can raise the potential.[1,2] To examine the correlation between CO formation and the potential rise, the kinetics for CO formation was examined in 0.5 M H_2SO_4 + 0.1 M HCOOH for a potential step from 1.4 to 0.4 V. The pre-electrolysis at 1.4 V was aimed to remove all adsorbed organic species from the electrode surface. The band intensities of CO_L, CO_B, and formate are plotted in Figure 5 as a function of time after stepping the potential to 0.4 V. The adsorption of formate is fast and reaches a maximum within 0.2 s (the time resolution used) and then decreases gradually probably due to the replacement by CO. A step-scan submillisecond time-resolved SEIRAS measurement revealed that formate coverage saturates within about 10 ms as in the case of other carboxylic acids on Au electrodes.[14] The adsorption of CO_B is also fast and saturates within 4 s. On the other hand, the adsorption of CO_L is much slower.

Since the oxidation of CO is negligibly slow at this low potential,[4] the rate of the CO_L formation is given as

$$\frac{d\theta_{CO\_L}}{dt} = k_{CO\_L}(1 - \theta_{CO\_L} - 2\theta_{CO\_B} - 2\theta_{formate})^n \quad (8)$$

assuming the Langmuir isotherm, where k_{CO_L} is the rate constant of the CO_L formation and n is the number of adjacent vacant sites required for CO_L formation. The prefactor 2 of $\theta_{formate}$ and θ_{CO_B} reflects the occupation of two surface sites for formate and CO_B. By integrating eq 8, CO_L coverage is represented as a function of time as

$$\theta_{CO\_L}(t) = (1 - 2\theta_{CO\_B} - 2\theta_{formate})[1 - \exp(-k_{CO\_L}t)] \quad (n = 1)$$

$$= (1 - 2\theta_{CO\_B} - 2\theta_{formate})\left\{1 - \frac{1}{[1 + (n-1)(1 - 2\theta_{CO\_B} - 2\theta_{formate})^{n-1}k_{CO\_L}t]^{1/(n-1)}}\right\} \quad (n > 1) \quad (9)$$

Assuming again the linear relationship between the band intensity and coverage and by treating $\theta_{CO\_B} + \theta_{formate}$ and k_{CO_L} as adjusting parameters, the best fit to the experimental data was obtained for $n = 2$ among 1, 2, 3, and 4 with $\theta_{CO\_B} + \theta_{formate} = 0.14$ and $k_{CO\_L} = 0.11\ s^{-1}$. The adjusted value for $\theta_{CO\_B} + \theta_{formate}$ is in reasonable agreement with that estimated from the band intensities of CO_B and formate by the procedure described before ($\theta_{CO\_B} + \theta_{formate} \sim 0.2$). Lu et al.[15] also obtained $n = 2$ from electrochemical measurements. Although the electrochemical measurements cannot distinguish the contributions from CO_L and CO_B, the two independent measurements are consistent because CO_B saturates quickly and its coverage is rather small.

Through systematic experiments at different potentials (0.4−0.8 V), the growth rate and the saturated intensity of the CO_L band were found to become smaller as the potential E is increased up to 0.6 V. No CO formation was observed at $E >$ 0.6 V probably because the CO formation is slower at higher potentials and is overwhelmed by oxidation.

3.5. Formic Acid Oxidation under Potential Sweep Conditions. The gradual increase in potential from 0.5 to 0.6 V in the potential oscillations (Figures 1a and 2a) can be ascribed to the slow kinetics of CO formation. However, the following sharp rise of potential from 0.6 to 0.8 V cannot be ascribed to CO formation because CO is oxidized at the high potentials (Figure 2c).

Since the increase of potential from 0.6 to 0.8 V is too fast to monitor with enough time resolution and signal-to-noise ratio, formic acid oxidation in the high potential range was examined in detail by linear sweep voltammetry in conjunction with time-resolved SEIRAS. Since voltammograms for formic acid oxidation greatly depend on CO coverage,[2f,16] the experiments were conducted at different CO coverages. The potential step technique used in Figure 5 allowed us to control CO coverage. The voltammograms in Figure 6 (panel a) were recorded after stepping the potential from 1.4 to 0.4 V and holding at this potential for 0, 20, and 100 s. To minimize the production of CO during the voltammetry, a relatively fast sweep rate of 100 mV s^{-1} was used in recording the voltammograms. Two peaks are found around 0.6 and 0.9 V in the voltammograms, which are denoted as peaks I and II, respectively, following earlier studies.[2f,16]

The intensities of the CO_L, CO_B, and formate bands taken from the sets of SEIRA spectra recorded simultaneously with the voltammograms are plotted as a function of the applied potential in Figure 6 (panels b, c, and d, respectively). The CO_L band decreases its intensity gradually with increasing the potential up to ~0.8 V and then faster at more positive potentials by oxidation. The CO_B band intensity decreases slightly at 0.4−0.6 V probably due to the conversion of CO_B to CO_L[4d] and keeps nearly constant at more positive potentials up to about 0.9 V, which is followed by a sharp decrease to zero together with the CO_L band. The potentials at which the CO_L and CO_B bands completely disappear are slightly shifted positively compared to the CO stripping in the pure electrolyte: Both CO_L and CO_B are completely oxidized at 0.8 V in the latter.[8b] The

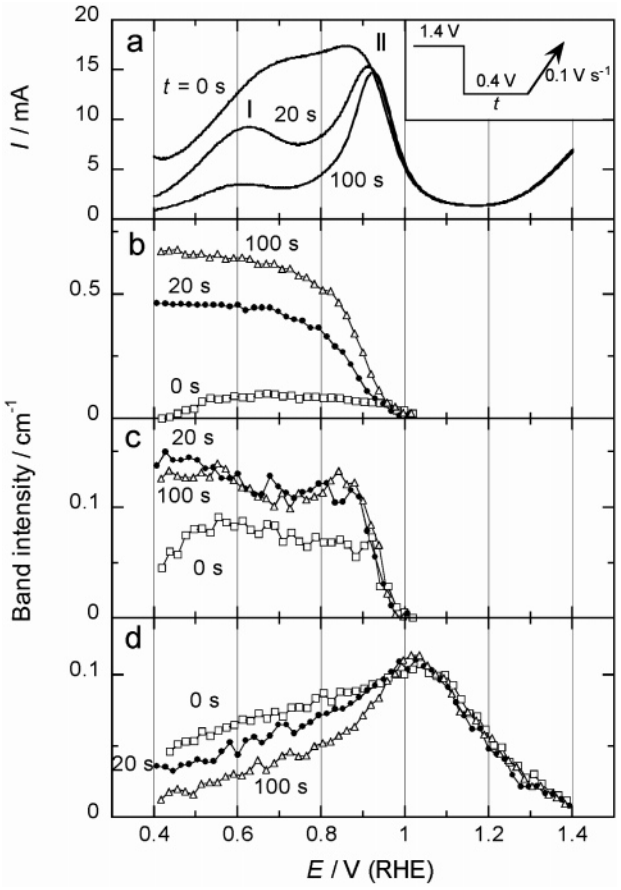

Figure 6. Linear sweep voltammograms in 0.5 M H_2SO_4 + 0.1 M HCOOH recorded at 0, 20, and 100 s after stepping the potential from 1.4 to 0.4 V at a sweep rate of 100 mV s^{-1} (a) and the integrated band intensities of CO_L (b), CO_B (c), and formate (d) taken from the three sets of time-resolved SEIRA spectra for the three waiting times.

positive shift of the oxidation (that is, the delay of oxidation) can be ascribed to the removal of oxygen species (water or OH) required for CO oxidation from the surface by formate. On the other hand, the formate band increases its intensity monotonically up to ~1 V and then decreases at more positive potentials due to the surface oxidation.[17] The potential dependence for each band in the potential region of 0.5−0.8 V is consistent with that observed during the potential oscillations (Figure 2).

A comparison of panels a and b in Figure 6 reveals that the oxidation current increases as CO coverage decreases and formate coverage increases. However, it should be noted that the oxidation current is not a simple function of the coverage of either CO or formate. For $t = 20$ and 100 s, for example, current decreases or remains constant in the potential range of 0.6−0.75 V despite the decrease in CO_L coverage. The observed currents are largely different in the three sets of experiments despite the small difference in formate coverage. These findings suggest that the oxidation of formic acid is a function of coverages of both formate and CO. We will return to this issue later.

3.6. Reaction Intermediate in the Direct Path, the Current Carrier. The most important issue for understanding the mechanism of the oscillations is to identify the reaction intermediate in the direct path. So far, COOH has long been assumed to be the reaction intermediate in the direct path.[1−4] COOH, if it exists, is expected to exhibit a strong C═O stretching band at 1600−1700 cm^{-1}. Unfortunately, the bands of water and formic acid in the solution interfer with this spectral range (Figure 1b). To remove this problem, we used dilute

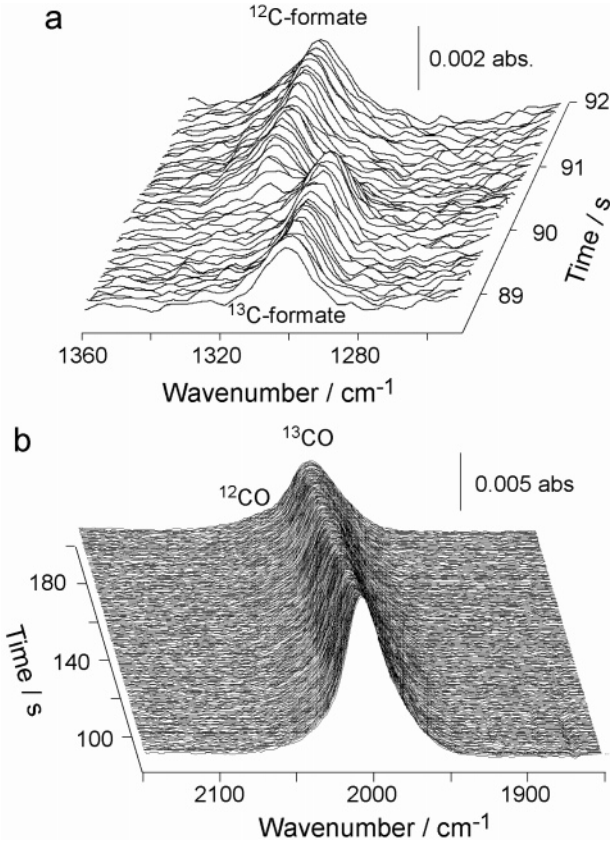

Figure 7. Time-resolved SEIRA spectra representing isotopic substitution of adsorbed formate (a) and CO_L (b) for a quick solution exchange from 0.5 M H_2SO_4 + 0.1 M $H^{13}COOH$ to 0.5 M H_2SO_4 + 0.1 M H^{12}-COOH at 0.6 V. The solution was changed at about 90 s after stepping the electrode potential from 0.05 to 0.6 V. Time resolution used was 80 ms.

(0.01−0.1 M) D_2O solutions of formic acid. Despite the complete elimination of the solution bands in this region, no signals attributable to COOH were detected.

In a previous paper,[8a] we suggested that adsorbed formate is a reactive intermediate in the direct path because the oxidation current increases as formate coverage increases (the corresponding data have been given in Figure 6). The experimental finding that potential drops in the oscillations when formate coverage reaches its maximum (Figure 2) also suggests formate being an intermediate (the potential drop indicates the activation of formic acid oxidation). This reaction mechanism is totally different from that assumed in the earlier studies, but identical with the well-established one for catalytic formic acid oxidation on metal and metal oxide surfaces in the gas phase (CO is also produced by a side reaction).[10,18,19] To examine the reaction mechanism further, a solution substitution experiment with isotope-labeled formic acids ($H^{12}COOH$ and $H^{13}COOH$) was carried out. The same tactics have been employed by Mrozek et al.[20] in a Raman study of formic acid oxidation on Rh and Ir electrodes to examine the contribution of the indirect path in the oxidation.

The experiment was started with 0.5 M H_2SO_4 + 0.1 M $H^{13}COOH$. After stepping the electrode potential from 0.1 to 0.6 V and waiting at this potential until the system reaches a stationary state (~90 s), the solution was quickly replaced with 0.5 M H_2SO_4 + 0.1 M $H^{12}COOH$ with use of a syringe. A set of 80-ms time-resolved SEIRA spectra collected during the solution exchange is shown in Figure 7. The symmetric O−C−O stretching mode of ^{13}C-formate at 1305 cm^{-1} is seen

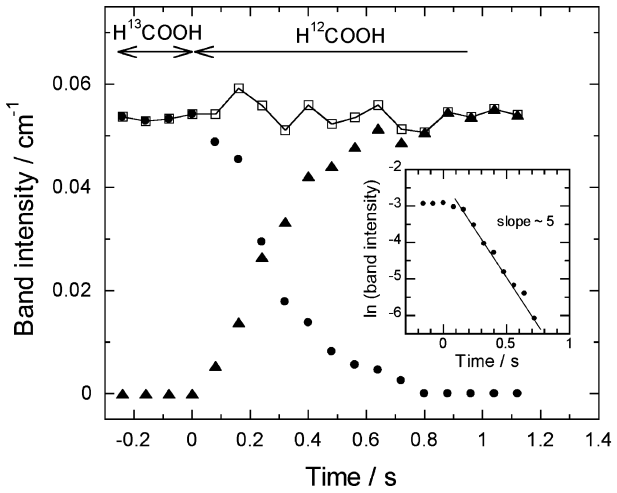

Figure 8. Integrated band intensities of ^{13}C-formate (closed circles), ^{12}C-formate (closed triangles), and the sum of them (open squares) taken from Figure 5a and plotted as a function of time after the isotopic solution exchange. Time was set to 0 when the ^{12}C-formate band appeared. The inset shows the semilogarithmic plot of the band intensity of ^{13}C-formate against time.

to be replaced by that of ^{12}C-formate at 1323 cm^{-1} within 1 s (panel a), while the isotopic substitution for CO_L is negligibly slow and the $^{12}CO_L$ band is observed only very weakly as a shoulder at the positive side of the $^{13}CO_L$ band at 2000 cm^{-1} even 100 s after the solution exchange (panel b). Negligible isotopic substitution was observed also for CO_B. The results show that the oxidation of CO is very slow under the stationary state and thus the indirect path through adsorbed CO scarcely contributes to formic acid oxidation at this potential.

The kinetics of the isotopic substitution for adsorbed formate was quantitatively analyzed by plotting the intensities of the ^{12}C- and ^{13}C-formate bands as a function of time. The result is shown in Figure 8. The ^{12}C-formate band (triangles) increases in intensity by consuming the ^{13}C-formate band (circles). The sum of the two bands (squares) is nearly constant during the experiment, implying that the adsorption of formate is fast enough and in equilibrium with the desorption. The decay of the ^{13}C-formate band can be approximated by the first-order reaction kinetics as is shown by the semilogarithmic plot of the intensity against time (Figure 8, inset). From the slope of the plot, the rate constant of ~5 s^{-1} is evaluated.

Two explanations are possible for the isotopic substitution of adsorbed formate. One is a simple adsorption/desorption as

$$\mathrm{HCOOH} + 2* \underset{k_{\mathrm{des}}}{\overset{k_{\mathrm{ad}}}{\rightleftharpoons}} \mathrm{HCOO(a)} + \mathrm{H^+} + \mathrm{e^-} \qquad (10)$$

where k_{ad} and k_{des} stand for the rate constants of adsorption and desorption, respectively. Another is the decomposition (oxidation) of adsorbed formate to CO_2 as

$$\mathrm{HCOO(a)} \xrightarrow{k_{\mathrm{decom}}} \mathrm{CO_2} + \mathrm{H^+} + \mathrm{e^-} + 2* \qquad (11)$$

No current flows in the former case, whereas current represented by eq 12 can flow in the latter case (i.e., $k_{decom} > k_{des}$).

$$i = 2FSk_{\mathrm{decom}}\theta_{\mathrm{formate}}\Gamma_{\mathrm{Pt}} \qquad (12)$$

by assuming the first-order reaction kinetics tentatively, where F is the Faraday constant, S is the real surface area of the electrode (10.8 cm^2), and Γ_{Pt} is the density of surface Pt atoms (1.3×10^{15} atoms cm^{-2} = 2.18×10^{-9} mol cm^{-2}, which

corresponds to 210 μC cm^{-2} for the monolayer hydrogen adsorption/desorption). Assuming $\theta_{formate} = 0.05-0.5$ (note 0.5 being the highest limit for formate), $i = 1-10$ mA is calculated from eq 12. The current of 3 mA observed during the isotopic substitution experiment is well in the expected range. This result strongly argues that formate is a reactive intermediate in the formic acid oxidation and the decomposition of formate to CO_2, eq 11, is rate determining.

Under the potentiostatic condition, the integrated intensity of the formate band observed is 0.053 cm^{-1} (Figure 8) and $\theta_{formate}$ is calculated to be 0.14 from the observed current of 3 mA through eq 12. These values were used in the rough estimation of the formate coverage mentioned above.

3.7. Mechanism of Potential Oscillations. The observed oscillations consist of an initial gradual and a following sharp rising parts (Figures 1a and 2a). The adsorption of CO can cause the initial gradual rise of potential from 0.5 to 0.6 V but not the following sharp rise up to 0.8 V, as discussed above. The potential range of the sharp rise corresponds to the positive side of peak I in the voltammograms (Figure 6), where current decreases as the potential increases. The negative slope in the potential range (negative differential resistance, NDR) has been suggested to raise the potential in the oscillations.[1,2] The process in the NDR region is autocatalytic in nature: The increase of potential suppresses the oxidation and leads to further increase of potential to maintain the applied current.

The adsorption of formate on Pt was not taken into account in the earlier models of oscillations.[1,2] The new finding of formate being a reactive intermediate forces us to revise the earlier models. In the framework assuming COOH as the reactive intermediate, several assumptions were made to explain the NDR. Strasser et al.[2i,j] ascribed the NDR to the inhibition of COOH adsorption by adsorbed OH. Schmidt et al.[2m] suggested the adsorption of supporting anions. Okamoto et al.[2f,g,k] proposed the inhibition of the direct path by adsorbed water. Wojtowicz et al.[2a] proposed a mechanism involving surface oxidation. All these effects could contribute to the oscillations, but would not be essential because the NDR can be explained reasonably without assuming any adsorbed species other than CO and formate as is discussed below. The model involving surface oxidation by Wojtowicz et al.[2a] is apparently ruled out in the present case since the potential range of the observed oscillations is below the onset potential of surface oxidation, 0.8 V.

In UHV studies of the decomposition reactions of formate and acetate on transition metal surfaces, it is well-known that adsorbed formate (or acetate) species themselves block each other's decomposition and are stabilized remarkably at high coverage.[19] Once the reaction is initiated at certain sites (e.g., steps and defects), it progresses autocatalytically, which is called surface explosion. The requirement for observing surface explosion is *local* coverage and rather independent of the global one. The stabilization occurs even at low coverages when the carboxylate species form islands or other species are coadsorbed, suggesting the necessity of vacant sites adjacent to the adsorbed caroboxylate species for their decomposition.[19] Bowker and coworkers[19c-e] explained the stabilization as that the frustrated rotation mode of adsorbed carboxylate through which it is decomposed is sterically hindered by the occupation of the adjacent sites by coadsorbates including itself. The nonlinear kinetics has been observed also in the CO/NO coadsorbed system.[21] The stabilization effect is expected to play an important role also in formic acid electrooxidation via adsorbed formate.

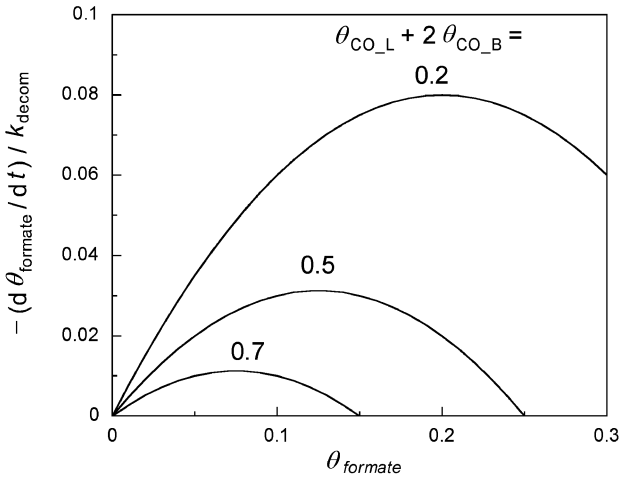

Figure 9. Formate-coverage dependence of the normalized formate decomposition rate $(-d\theta_{formate}/dt)/k_{decom}$ calculated with the second-order rate eq 13 for constant CO coverages $(=\theta_{CO\_L} + 2\theta_{CO\_B})$ of 0.2, 0.5, and 0.7.

Two kinetic models have been proposed to explain surface explosions; second-order and circular island models.[19a,c-e] The former assumes random occurrence of the reaction, whereas the latter assumes islandlike occurrence of the reaction. By using the second-order kinetic model, for the sake of simplicity, the voltammetric behavior of formic acid can be simulated as follows.

The second-order rate equation is given as

$$-\frac{d\theta_{formate}}{dt} = k_{decom}\theta_{formate}(1 - 2\theta_{formate} - \theta_{CO\_L} - 2\theta_{CO\_B}) \quad (13)$$

by modifying the original rate equation[19] to fit the present definition of coverage and to include coadsorbed CO, where the second term in the right-hand side shown in parentheses corresponds to the coverage of vacant surface site. The normalized rate of formate decomposition, $-(d\theta_{formate}/dt)/k_{decom}$, calculated by eq 13 is plotted in Figure 9 as a function of formate coverage for $\theta_{CO\_L} + 2\theta_{CO\_B} = 0.2$, 0.5, and 0.7, which correspond to the experimental conditions for $t = 0$, 20, and 100 s, respectively, in the voltammetric measurements shown in Figure 6. The plot shows that (i) the reaction rate is remarkably decreased as CO coverage increases and (ii) the $\theta_{formate}$ dependence of the reaction rate changes from positive to negative by an increase of $\theta_{formate}$ crossing $\theta_{formate} = (1 - \theta_{CO\_L} - 2\,\theta_{CO\_B})/4$. Note that the calculated curves can be correlated with the voltammograms in the peak I region since oxidation current is proportional to the decomposition rate of formate and formate coverage increases almost linearly with potential E without changing CO coverage so significantly (Figure 6). Although the Butler-Volmer type potential dependence of the rate constant k_{decom} is neglected here, the peak I region in the voltammograms is well reproduced. The model calculation predicts that the NDR appears at $\theta_{formate}$ larger than 0.2, 0.125, and 0.08 for $\theta_{CO\_L} + 2\theta_{CO\_B} = 0.2$, 0.5, and 0.7, respectively. Since the $\theta_{formate}$ estimated from the band intensity is 0.08-0.2 at 0.4-0.8 V in the potential sweep experiments (Figure 6), the NDR should not appear at low CO coverage. This prediction is consistent with the observation.

The calculation also shows that the reaction rate is nearly proportional to $\theta_{formate}$ in a relatively wide $\theta_{formate}$ range for small θ_{CO}. Therefore, the assumption of the first-order rate equation used in analyzing the isotopic substitution experiment, eq 12,

is reasonable under the experimental conditions used ($\theta_{CO\_L} \sim 0.15$ and $\theta_{CO\_B} \sim 0.1$). By analyzing the isotopic substitution experiment shown in Figure 7 using the second-order rate equation, eq 13, the rate constant k_{decom} for the second-order rate equation were roughly estimated to be $\sim 10\ s^{-1}$. From rate constant and the current (3 mA), formate coverage is calculated to be ~0.14, which is identical with that estimated by the first-order rate equation.

We have demonstrated that the NDR, the origin of the sharp rise of potential in the oscillation, is well explained by the nonlinear kinetics of formate decomposition. It should be noted that Wojtowicz et al.[2a] proposed nonlinear rate equations similar to the second-order and circular island models for surface explosion to explain potential oscillations in formic acid electrooxidation. The authors have predicted mathematically that these nonlinear rate equations can simulate the electrochemical oscillations, although the chemical processes assumed were totally different from the observation in the present study. We will report in a separate paper[12] that the potential oscillations can actually be simulated by employing the observed reaction scheme and the rate eq 13. Current oscillations in potentiostatic electrooxidation of formic acid can be explained by the same scenario as well.[22]

4. Conclusion

Time-resolved ATR-SEIRAS was employed successfully to monitor the surface dynamic processes in the potential oscillations that occur in the galvanostatic formic acid oxidation on a Pt electrode. Associated with the temporal oscillations of potential, the band intensities of adsorbed CO_L and formate oscillated, while that of the CO_B was scarcely changed. By using isotope-labeled formic acids ($H^{12}COOH$ and $H^{13}COOH$), it was confirmed that formic acid is oxidized to CO_2 through adsorbed formate and this direct path consumes most of the applied current. These findings forced us to revise the existing models of the oscillation that assume $\underline{C}OOH$ being the reactive intermediate. The central part of the new mechanism proposed in the present study is that the rate of formic acid oxidation is represented by a nonlinear function of the coverages of both formate and CO. The reaction rate increases and then decreases with increasing formate coverage. The role of CO is 2-fold: the inhibition of formic acid chemisorption yielding formate and the suppression of the decomposition of formate to CO_2 by blocking adjacent surface sites required for the formate decomposition. The slow CO_L formation raises the potential gradually and the nonlinear kinetics of the direct path through formate raises the potential further to the high limiting potential. The oxidative removal of CO at the high potentials accelerates the decomposition of formate, resulting in the sudden drop of potential. This cycle repeats to yield sustained potential oscillates.

Acknowledgment. This work was supported by the Ministry of Education, Culture, Sports, Science and Technology of Japan (Grant-in-Aid for Basic Research No. 14205121 and for Scientific Research on Priority Areas 417), Japan Science and Technology Agency, Research Institute of the Innovative Technology for the Earth, and the Asahi Glass Foundation. Y.M. and H.O. acknowledge the support by the Research Institute for Science and Technology of Tokyo Denki University (Grants Q01M-08 and Q02M-07).

References and Notes

(1) (a) Wojtowicz, J. In *Modern Aspects of Electrochemistry*; Bockris, J. O.-M., Conway, B. E., Eds.; Plenum Press: New York, 1972; Vol. 8. (b) Hudson, J. L.; Tsotsis, T. T. *Chem. Eng. Sci.* **1994**, *49*, 1493. (c) Koper, M. T. M. In *Advances in Chemical Physics*; Prigogine, I., Rice, S. A., Eds.; Wiley: New York, 1996; Vol. 92, p 161. (d) Krischer, K. In *Modern Aspects of Electrochemistry*; Conway, B. E., Bockris, J. O. M., White, R. E., Eds.; Kluwer Academic/Plenum: New York, 1999; Vol. 32, p 1. (e) Krischer, K.; Mazouz, N.; Grauel, P. *Angew. Chem., Int. Ed.* **2001**, *40*, 850.

(2) (a) Wojtowicz, J.; Marincic, N.; Conway, B. E. *J. Chem. Phys.* **1968**, *48*, 4333. (b) Schell, M.; Albahadily, F. N.; Safar, J.; Xu, Y. *J. Phys. Chem.* **1989**, *93*, 4806. (c) Anastasijevic, N. A.; Baltruschat, H.: Heitbaum, J. *J. Electroanal. Chem.* **1989**, *272*, 89. (d) Raspel, F.; Nichols, R. J.; Kolb, D. M. *J. Electroanal. Chem.* **1990**, *286*, 279. (e) Albahadily, F. N.; Schell, M. *J. Electroanal. Chem.* **1991**, *308*, 151. (f) Okamoto, H. *Electrochim. Acta* **1992**, *37*, 37. (g) Okamoto, H. *Chem. Phys. Lett.* **1996**, *248*, 289. (h) Raspel, F.; Eiswirth, M. *J. Phys. Chem.* **1994**, *98*, 7613, (i) Strasser, P.; Lübke, M.; Raspel, F.; Eiswirth, M.; Ertl, G. *J. Chem. Phys.* **1997**, *107*, 979. (j) Strasser, P.; Eiswirth, M.; Ertl, G. *J. Chem. Phys.* **1997**,*107*, 991; (k) Naito, M.; Okamoto, H.; Tanaka, N. *Phys. Chem. Chem. Phys.* **2000**, *2*, 1193. (l) Chen, S.; Noles, T.; Schell, M. *J. Phys. Chem. A* **2000**, *104*, 6791. (m) Schmidt, T. J.; Grgur, B. N.; Markovic, N. M.; Ross, P. N., Jr. *J. Electroanal. Chem.* **2001**, *500*, 36.

(3) Capon, A.; Parsons, R. *J. Electroanal. Chem.* **1973**, *44*, 1. Capon, A.; Parsons, R. *J. Electroanal. Chem.* **1973**, *44*, 239. Capon, A.; Parsons, R. *J. Electroanal. Chem.* **1973**, *45*, 205.

(4) (a) Kunimatsu, K. *J. Electroanal. Chem.* **1986**, *213*, 149. (b) Kunimatsu, K.; Kita, H. *J. Electroanal. Chem.* **1987**, *218*, 155. (c) Corrigan, D. S.; Weaver, M. J. *J. Electroanal. Chem.* **1988**, *241*, 143. (d) Iwashita, T.; Xia, X.; Herrero, E.; Leiss, H.-D. *Langmuir* **1996**, *12*, 4260.

(5) (a) Nichols, R. J. In *Adsorption of Molecules at Metal Electrodes*; Lipkowski, J., Ross, P. N., Eds.; VCH: New York, 1992; p 347. (b) Iwashita, T.; Nart, F. C. *Prog. Surf. Sci.* **1997**, *55*, 271.

(6) (a) Osawa, M. *Bull. Chem. Soc. Jpn.* **1997**, *70*, 2861. (b) Osawa, M. In *Near-Field Optics and Surface Plasmon Polaritons*; Kawata, S., Ed.; Springer: Berlin, Germany, 2001; p 163. (c) Osawa, M. In *Vibrational Spectroscopy*; Charmers, J., Griffiths, P. R., Eds.; Chichester, 2002; Vol. 1, p 785.

(7) (a) Osawa, M.; Ataka, K.; Yoshii, K.; Yotsuyanagi, T. *J. Electron Spectrosc. Relat. Phenom.* **1993**, *64/65*, 371. (b) Ataka, K.; Yotsuyanagi, T.; Osawa, M. *J. Phys. Chem.* **1996**, *100*, 10664.

(8) (a) Miki, A.; Ye, S.; Osawa, M. *Chem. Commun.* **2002**, 1500. (b) Miki, A.; Ye, S.; Senzaki, T.; Osawa, M. *J. Electroanal. Chem.* **2004**, *563*, 23.

(9) Osawa, M.; Ataka, K.; Yoshii, K.; Nishikawa, Y. *Appl. Spectrosc.* **1993**, *47*, 1497.

(10) (a) Columbia, M. R.; Carbtree, A. M.; Thiel, P. A. *J. Am. Chem. Soc.* **1992**, *114*, 1231. (b) Columbia, M. R.; Crabtree, A. M.; Thiel, P. A. *J. Electroanal. Chem.* **1993**, *345*, 93.

(11) Kunimatsu, K.; Samant, M. G.; Seki, H.; Philpott, M. R. *J. Electroanal. Chem.* **1988**, *243*, 203.

(12) Mukouyama, Y.; Kikuchi, M.; Samjeské, G.; Osawa, M.; Okamoto, H. To be submitted for publication.

(13) Leung, L.-W. H.; Wieckowski, A.; Weaver, M. J. *J. Phys. Chem.* **1988**, *92*, 6985.

(14) (a) Noda, H.; Ataka, K.; Wan, L.-J.; Osawa, M. *Surf. Sci.* **1999**, *427−428*, 190. (b) Noda, H.; Wan, L.-J.; Osawa, M. *Phys. Chem. Chem. Phys.* **2001**, *3*, 3336.

(15) Lu, G.-Q.; Crown, A.; Wieckowski, A. *J. Phys. Chem. B* **1999**, *103*, 9700.

(16) Okamoto, H.; Kon, W.; Mukouyama, Y. *J. Phys. Chem. B* **2004**, *108*, 4432.

(17) Samjeské, G.; Miki, A.; Ye, S.; Osawa, M. To be submitted for publication.

(18) Columbia, M. R.; Thiel, P. A. *J. Electroanal. Chem.* **1994**, *369*, 1.

(19) (a) Falconer, J. L.; Madix, R. J. *Surf. Sci.* **1974**, *46*, 473. (b) Madix, R. J.; Falconer, J. L.; Suszko, A. M. *Surf. Sci.* **1976**, *54*, 6620. (c) Li, Y.; Bowker, M. *Surf. Sci.* **1993**, *285*, 219. (d) Sharpe, R. G.; Bowker, M. *J. Phys. Condens. Matter* **1995**, *7*, 6379. (e) Bowker, M.; Morgan, C.; Couves, J. *Surf. Sci.* **2004**, *555*, 145.

(20) Mrozek, M. F.; Luo, H.; Weaver, M. J. *Langmuir* **2000**, *16*, 8463.

(21) (a) Lesley, M. W.; Schmidt, L. D. *Surf. Sci.* **1984**, *155*, 215. (b) Fink, T.; Dath, J.-P.; Bassett, M. R.; Imbihl, R.; Ertl, G. *Surf. Sci.* **1991**, *245*, 96. (c) Zagatta, G.; Müller, H.; Wehmeyer, O.; Brandt, M.; Böwering, N.; Heinzmann, U. *Surf. Sci.* **1994**, *307−309*, 199.

(22) Samjeské, G.; Osawa, M. *Angew. Chem., Int. Ed.* **2005**, *44*, 5694−5698.